Available online at www.sciencedirect.com
ScienceDirect
Trans. Nonferrous Met. Soc. China 24(2014) 1866−1873
Transactions of Nonferrous Metals Society of China
www.tnmsc.cn

Improved spatial resolution in soil moisture retrieval at arid mining area using apparent thermal inertia

Shao-gang LEI[1], Zheng-fu BIAN[1], John L. DANIELS[2], Dong-lie LIU[3]

1. State Key Laboratory for GeoMechanics and Deep Underground Engineering, China University of Mining and Technology, Xuzhou 221116, China;
2. Department of Civil Engineering, University of North Carolina at Charlotte, Charlotte, 28223, USA;
3. School of Environment Sciences and Spatial Informatics, China University of Mining and Technology, Xuzhou 221116, China

Received 10 July 2013; accepted 6 January 2014

Abstract: A surface soil moisture model with improved spatial resolution was developed using remotely sensed apparent thermal inertia (ATI). The model integrates the surface temperature derived from TM/ETM+ image and the mean surface temperature from MODIS images to improve the spatial resolution of soil temperature difference based on the heat conduction equation, which is necessary to calculate the ATI. Consequently, the spatial resolution of ATI and SMC can be enhanced from 1 km to 120 m (TM) or 60 m (ETM+). Moreover, the enhanced ATI has a much stronger correlation coefficient (R^2) with SMC (0.789) than the surface reflectance (0.108) or the ATI derived only from MODIS images (0.264). Based on the regression statistics of the field SMC measurement and enhanced ATI, a linear regression model with an RMS error of 1.90% was found.
Key words: soil water content; soil temperature difference; thermal inertia; remote sensing; spatial resolution

1 Introduction

Measurement of soil moisture content (SMC) is fundamental to many investigations in civil engineering, hydrology and other eco-environmental fields [1]. Advanced remote sensing (RS) technology has been widely employed to monitor soil moisture for its convenience and high efficiency [2,3]. Many indicators derived from the non-radar spectra range are known for soil moisture estimation, e.g. thermal inertia [4], soil reflectance [5], and wetness index derived from tasseled cap transformation [6]. In particular, thermal inertia has been utilized widely, which is a function of the soil conductivity, density and heat capacity, and describes the impedance to the variation of soil temperature. Therefore, inverse methods that make use of thermal inertia to retrieve the soil moisture are applied [4]. Then, it is critical to obtain the soil temperature difference with higher spatial resolution. However, only a few satellite sensors can provide the diurnal soil temperature difference, such as the MODIS or NOAA/AVHRR sensor [7,8]. The deficiency is that the soil temperature difference and soil moisture retrieved from those images are at a moderate spatial resolution of 1 km. Although, the Landsat TM/ETM+ images have much higher spatial resolution than the MODIS images, they have not been used with ATI method to predict soil moisture for three reasons.

Firstly, Landsat TM/ETM+ images cannot provide the day−night soil temperature difference. For this reason, CHANG [8] obtained the soil temperature difference from MODIS images to predict soil moisture, but the spatial resolution is 1 km, which could not be applied at small areas. HEJMANOWSKA and MULARZ only used one phase of surface soil temperature derived from the thermal infrared band of the TM image to retrieve soil moisture with the ATI method [9].

Secondly, it is known that the soil temperature or the day−night soil temperature difference is a function of

Foundation item: Project (2013CB227904) supported by the National Basic Research Program of China; Project (2012QNB09) supported by the Fundamental Research Funds for the Central University, China; Project (NCET-12-0956) supported by the Program for New Century Excellent Talents
Corresponding author: Shao-gang LEI; Tel/Fax: +86-516-83590159; E-mail: lsgang@126.com
DOI: 10.1016/S1003-6326(14)63265-9

depth and time [10]. In other words, the soil moisture is also a function of soil depth and time. The soil temperature derived from satellite images is often the ground surface temperature. Therefore, the surface temperature from RS must be converted to corresponding soil depth.

Thirdly, the soil temperature difference is often simply taken as the difference value between the highest and lowest temperatures. However, the temperature obtained from TM image is neither the highest temperature nor the lowest temperature. Consequently, the temperature obtained from the TM image is lower than the highest temperature, and a temperature conversion must be conducted to get a more accurate daily highest temperature.

The objective of this study is therefore to model the soil temperature difference at shallow depth to estimate soil moisture at a higher spatial resolution by integrating TM/ETM+ images and the ATI method. It is significant for the other higher spatial resolution images with infrared bands, if the aforementioned three limitations can be resolved.

2 Methods

2.1 Obtaining apparent thermal inertia

To avoid complicated calculation for thermal inertia, PRICE [4] presented an apparent thermal inertia (ATI, β), which is a function of surface albedo (A) and soil temperature difference (ΔT), defined by Eq. (1). MINACAPILLI et al [11] predicted the surface soil moisture from the ATI with an acceptable level of accuracy for practical purposes at a laboratory scale. Therefore, it is very promising for regional application, if the ATI can be obtained using remote sensing.

$$\beta=(1-A)/\Delta T \tag{1}$$

Normally, there is a positive correlation between soil moisture content (SMC, η) and ATI, where the ground is bare or sparsely vegetated. It can be expressed as a linear model ($\eta=a\cdot\beta+b$), logarithm model ($\eta=a\cdot\ln\beta+b$) or exponential model ($\eta=a\cdot e^{b\cdot\beta}$). Parameters a and b are statistic coefficients. For Landsat TM/ETM+ images, the A can be calculated using Eq. (2) [12].

$$A=0.606\rho_{ch.1}+0.286\rho_{ch.2}+0.244\rho_{ch.3}+0.164\rho_{ch.4} \tag{2}$$

where $\rho_{ch.1}$, $\rho_{ch.2}$, $\rho_{ch.3}$ and $\rho_{ch.4}$ refer to the surface reflectance from bands 1, 2, 3 and 4, which can be obtained using FLAASH model in ENVI (Environment for Visualizing Images) software.

2.2 Modeling soil temperature difference

Soil temperature can be predicted with the aid of ground surface temperature based on the one dimensional heat conduction equation [12], expressed as

$$\frac{\partial T}{\partial t}=\frac{\partial}{\partial z}\left(\alpha\frac{\partial T}{\partial z}\right) \tag{3}$$

where T (K) is the soil temperature at depth of z (cm) and time t (h); α is the soil thermal diffusivity (cm^2/h).

The heat conduction equation can be solved by two boundary conditions. The first one expresses that the surface soil temperature is equal to air temperature, which varies according to a sinusoidal function [12]. The second boundary condition expresses that the soil temperature is constant and equal to the mean air temperature at deep position [13]. Moreover, the solution has been improved for more accurate prediction [14]. Firstly, the symmetry model was modified to asymmetry through the adjustment of cosine function. Secondly, the model is improved to be continuous across multiple days. Thirdly, the improved model takes into account the daily variation of the relationship between the air and soil temperature amplitude. The improved soil temperature model is developed as Eq. (4). It can be used to predict soil temperature at different depths and time. For example, LEI et al [14] predicted the soil temperature at depths of 4.5 cm, 9.5 cm and 18.5 cm, respectively, at highway U.S.70, near Clayton, North Carolina, USA. The RMS error of the predicted soil temperature was lower than 1.5 K.

$$T_{z,t}=T_{\mathrm{Smean}}+\frac{1}{2}(T_{\mathrm{Am1}}-T_{\mathrm{Am}})\cdot\exp(-z\cdot\sqrt{\frac{\pi}{\alpha\cdot p}})+A_z\cdot K(t) \tag{4}$$

where $T_{z,t}$ is the soil temperature at depth of z (cm) and time of t (h); p is the period, normally 24 h; T_{Smean} is the mean surface soil temperature; A_z is the soil temperature amplitude defined as half of the temperature difference ($0.5\Delta T$) at depth of z; $T_{\mathrm{Am1}}-T_{\mathrm{Am}}$ is the mean surface temperature difference between adjacent days. The thermal diffusivity α varies with soil types. For sand soil, the α was set as 33.12 cm^2/h [15]. The $K(t)$ is a piecewise periodic function, expressed as Eq. (5) [14], when t is between the time of the lowest temperature ($t_{\min}$) and the highest temperature ($t_{\max}$). The $t_{\min}$ and $t_{\max}$ can be obtained from meteorological data. In Eq. (5), the P_1 is $2(t_{\max}-t_{\min})$, and the mod is a function that returns the remainder after a number is divided.

$$K(t)=-\cos\left[\frac{2\pi}{P_1}\cdot(\mathrm{mod}((t-\frac{z}{2}\sqrt{\frac{p}{\pi\alpha}}),24)-t_{\min})\right] \tag{5}$$

The surface soil temperature amplitude (A_0) is expressed as

$$A_0 = \frac{T_{0,t} - T_{\text{Smean}} - \frac{1}{2}(T_{\text{Am1}} - T_{\text{Am}})}{K(t)} \quad (6)$$

The T_{TM} derived from TM/ETM+ image can substitute for $T_{0,t}$. Then, a soil temperature difference model can be expressed as

$$\Delta T = 2A_0 \cdot \exp(-z\sqrt{\frac{\pi}{\alpha \cdot p}})$$

$$= 2\frac{T_{\text{TM}} - T_{\text{Smean}} - \frac{1}{2}(T_{\text{Am1}} - T_{\text{Am}})}{K(t)} \cdot \exp(-z\sqrt{\frac{\pi}{\alpha \cdot p}}) \quad (7)$$

Thereby, the spatial resolution of ΔT can be enhanced from 1 km to 120 m (TM) or 60 m (ETM+).

2.3 Deriving surface temperature from TM/ETM+ and MODIS images

Mono-window algorithm shown as Eq. (8) is a very useful method to derive surface temperature from the thermal infrared band of TM/ETM+ image [16].

$$T_{\text{TM}} = \{a(1-c_6-d_6)+[b(1-c_6-d_6)+c_6+d_6]I_6 - d_6T_{\text{a}}\}/c_6 \quad (8)$$

where a and b are constant, equal to −67.355351 and 0.458606 respectively; $c_6=\varepsilon_6\tau_6$, $d_6=(1-\varepsilon_6)[1+(1-\varepsilon_6)\tau_6]$; ε_6 is the surface emissivity; T_{a} is the average atmosphere temperature (K), equal to $16.01101+0.926211T_0$; T_0 is the mean air temperature; I_6 is the radiation brightness temperature of the sixth band [17]; τ_6 is the atmospheric transmittance, which can be derived from MODIS images [18]. The ε_6 can be obtained based on the relationship between surface emissivity and normalized difference vegetation index [19].

MODIS provides two kinds of daily surface temperature products with 1 km resolution from Aqua and Terra satellites, which are freely available. WANG [20] found that the surface temperature from those products is very accurate, with an error lower than 1 K. Normally, the daytime image is obtained around 14:00 PM, and the nighttime image is at 3:00 AM, which are close to the time of daily highest and lowest temperatures, respectively. Thus, the mean temperature T_{Smean} can be simply taken as the average of the highest and lowest temperatures from the MODIS temperature products.

Figure 1 shows the temperature frequency of the study area during daytime and nighttime. It indicates that the temperature range of daytime is wider than that of nighttime. That is to say, the variation of daytime temperature is the primary effect on the variation of mean temperature.

2.4 Study area and dataset

The study area is in the Shendong arid coal mining area located at the border of Shanxi Province and Inner Monogolia, China (Fig. 2). Three coal mines were selected as the investigation areas, i.e. Bulianta, aliuta

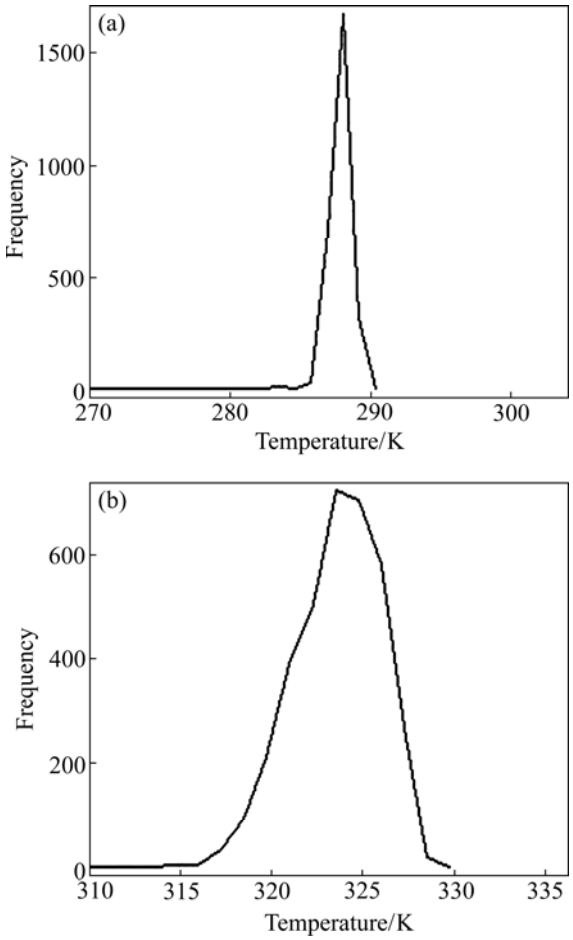

Fig. 1 Temperature frequency at daytime (a) and nighttime (b) from MODIS

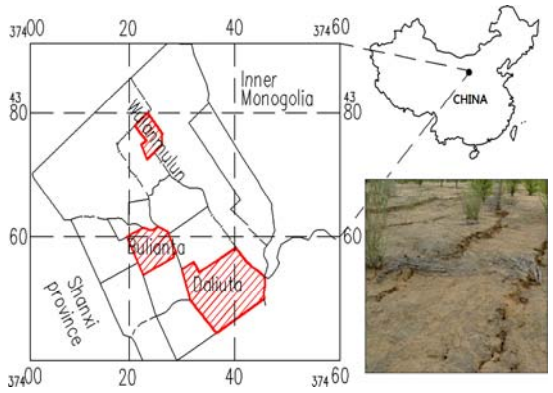

Fig. 2 Location of study area and ground surface of mining area

and Wulanmulun mine. The total study area is about 250 km^2; and the elevation is between 1000 m to 1500 m. The average annual rainfall is 436.7 mm, about 70% of which occurs in August and September. The primary soil type is sand with a large temperature difference between day and night. The ground surface is sparsely vegetated area, which is suitable for the ATI method to measure soil moisture. The reason for choosing this area is also to detect the ground subsidence impacts on the spatial difference of soil moisture, and verify the feasibility of the proposed remotely sensed ATI method for practical application.

A Landsat TM image on July 5th 2005 with spectral bands of 30 m spatial resolution and one infrared band of 120 m spatial resolution was preprocessed by geometrical- and atmosphere-corrections, using ENVI. Several daily MODIS temperature products including Aqua and Terra images around July 5th 2005 were geo-referenced to the TM image.

The field volumetric soil moisture content was measured by a portable wet sensor, while remote sensing images were taken on July 5th 2005. The wet sensor (type: WET-2) designed by Delta-T Devices Ltd. can convert the measured dielectric properties into water content over the full range, 0−80%. The sensor was calibrated for the sand soil of study area using a simple mixing formula that relates water content to the measured permittivity of the soil (referring to Delta-T WET-2 manual, 2005). To determine the optimal depth for soil moisture retrieval, the sampling depths of each location were at 10 cm, 20 cm and 40 cm.

The procedure for one field soil moisture sampling is as follows. Firstly, an area of 30 m×30 m was selected, where the surface cover is homogenizing and easy for excavating. A portable GPS was also used for positioning the center of sampling area. Secondly, five holes were evenly dug in the sample area and the soil moistures were measured at depths of 10 cm, 20 cm and 40 cm for each hole; three repeated readings were recorded with wet sensor and averaged for each depth at each hole. Thirdly, the average readings of the five holes at each depth were averaged again for one sample area. In total, 46 samples with three different depths were investigated inside and outside of the mined area (Fig. 3).

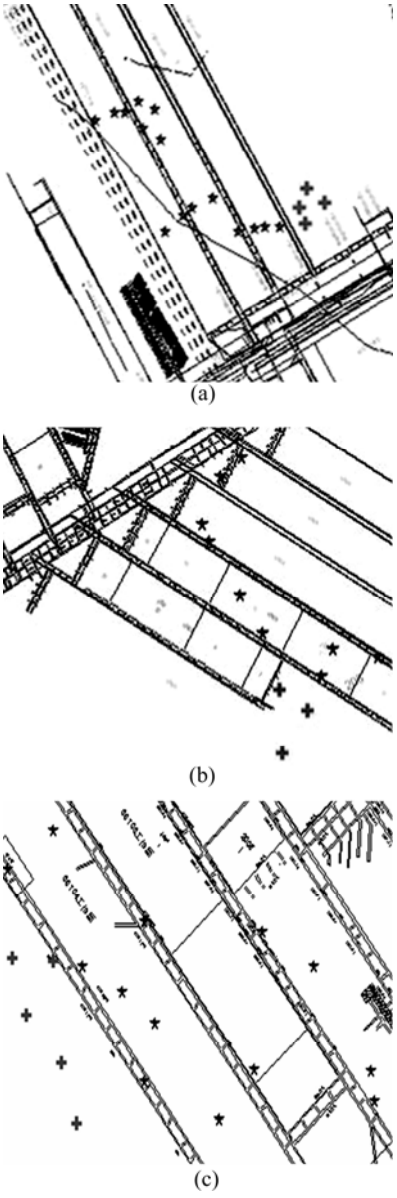

Fig. 3 Location of soil moisture samples at Bulianta (a), Daliuta (b) and Wulanmulun (c) mine

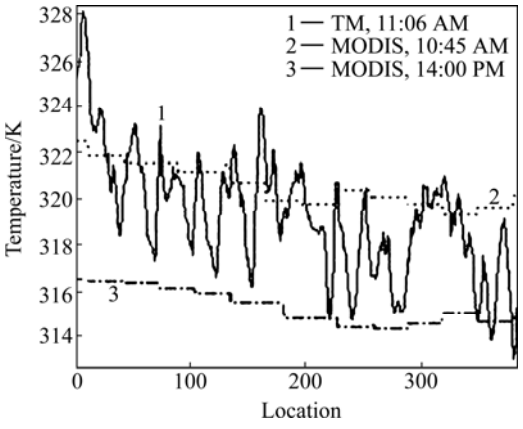

Fig. 4 Spatial profiles of surface temperature derived from MODIS and TM image (The unit of horizontal axis is pixel (30 m per pixel))

3 Results and discussion

3.1 Soil temperature from satellite images

Soil temperature can be derived based on the above algorithms. Figure 4 gives three random profiles of surface temperature derived from TM and MODIS images. The length of the profile is 12 km. It shows that

the temperature profile from TM image contains much more detailed spatial variations than that from MODIS images. It also demonstrates that the temperature at 14:00 PM from MODIS is higher than the morning temperature from MODIS and TM images, which is in accordance with the daily change of temperature.

Moreover, Fig. 5 illustrates that the spatial variation of daytime temperature is greater than that of nighttime temperature and mean temperature at a profile length of 250 km. By contrast, the mean temperature has a very low spatial variance at this spatial scale. It indicates that the spatial variance of daily temperature is mainly governed by the highest temperature. Therefore, the spatial resolution of the mean temperature in Eq. (7) is relatively not critical compared with T_{TM}.

In addition, the soil temperature difference at depth of 10 cm was derived based on Eq. (7). Figure 6 shows a profile of soil temperature difference derived only from MODIS images (on surface), and TM+MODIS images (at depth of 10 cm), respectively. It is clear that the soil temperature difference from TM+MODIS images has more detailed spatial variation information than that only from MODIS. In addition, the mean temperature difference at surface is much higher than that at depth of 10 cm.

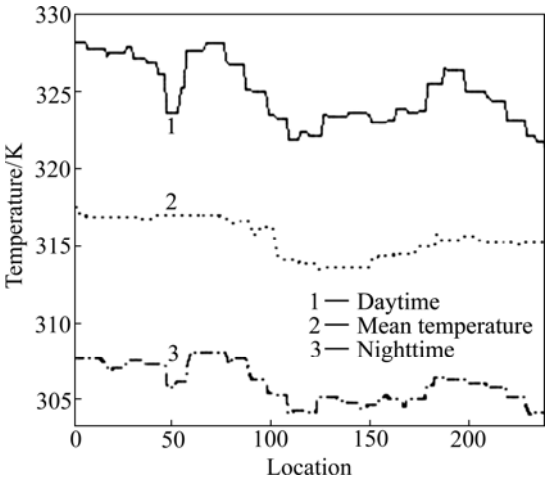

Fig. 5 Spatial profiles of surface temperature of study area at daytime, nighttime and mean temperature from MODIS (The horizontal axis unit is pixel (1 km per pixel))

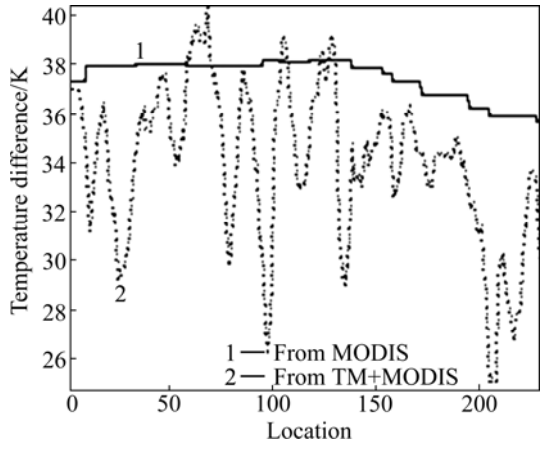

Fig. 6 Spatial profile of soil temperature difference derived only from MODIS on surface and from TM+MODIS at depth of 10 cm (The horizontal axis unit is pixel (30 m per pixel))

3.2 Relationship between improved apparent thermal inertia and soil moisture

As mentioned previously, the wetness index and soil reflectance also relate to soil moisture [5,6]. In an attempt to find a proper indicator of SMC, the wetness index, surface reflectance, and ATI_MODIS are also acquired to compare with ATI_TM. The ATI_MODIS is the ATI derived only from MODIS images with lower spatial resolution. ATI_TM is the ATI with aid of TM image and soil temperature difference model at higher spatial resolution. Figure 7 shows the relationships between different indicators and actual in situ SMC at depth of 10 cm. It is found that ATI_TM has the highest correlation with SMC (R^2=0.789), compared to ATI_MODIS (R^2=0.264), wetness index (R^2=0.310), and surface reflectance (R^2=0.108). Consequently, it is found that higher spatial resolution of soil temperature difference contributes to discover the correlation of SMC and ATI.

Additionally, the correlation of ATI_TM and SMC at depths of 10 cm, 20 cm and 40 cm were analyzed respectively and are presented in Table 1. The strongest correlation was observed at depth of 10 cm. The correlation is expected to decrease with increasing depth, because the study area is located in an arid to semi-arid region, with deep and intermitted groundwater. Most of the shallow soil water comes from dew and occasional rainfall. In addition, the satellite sensor is good at detecting the ground surface to a limited depth.

3.3 Soil moisture estimation and error analysis

The field samples of SMC and corresponding ATI derived from TM image were regressed. Table 2 presents the four kinds of regression models. It is observed that the linear model has a stronger fitting degree than the logarithm model, power model or exponential model. Figure 8 illustrates that the SMC varies with ΔT based on the linear model, while the A is set as 0.12. It is found that the lower the ΔT, the greater the difference of SMC, and vice versa. Therefore, the improved soil temperature difference model will improve the accuracy of the SMC, especially for the area with lower ΔT. Further statistics analysis indicated that the linear model has the lowest

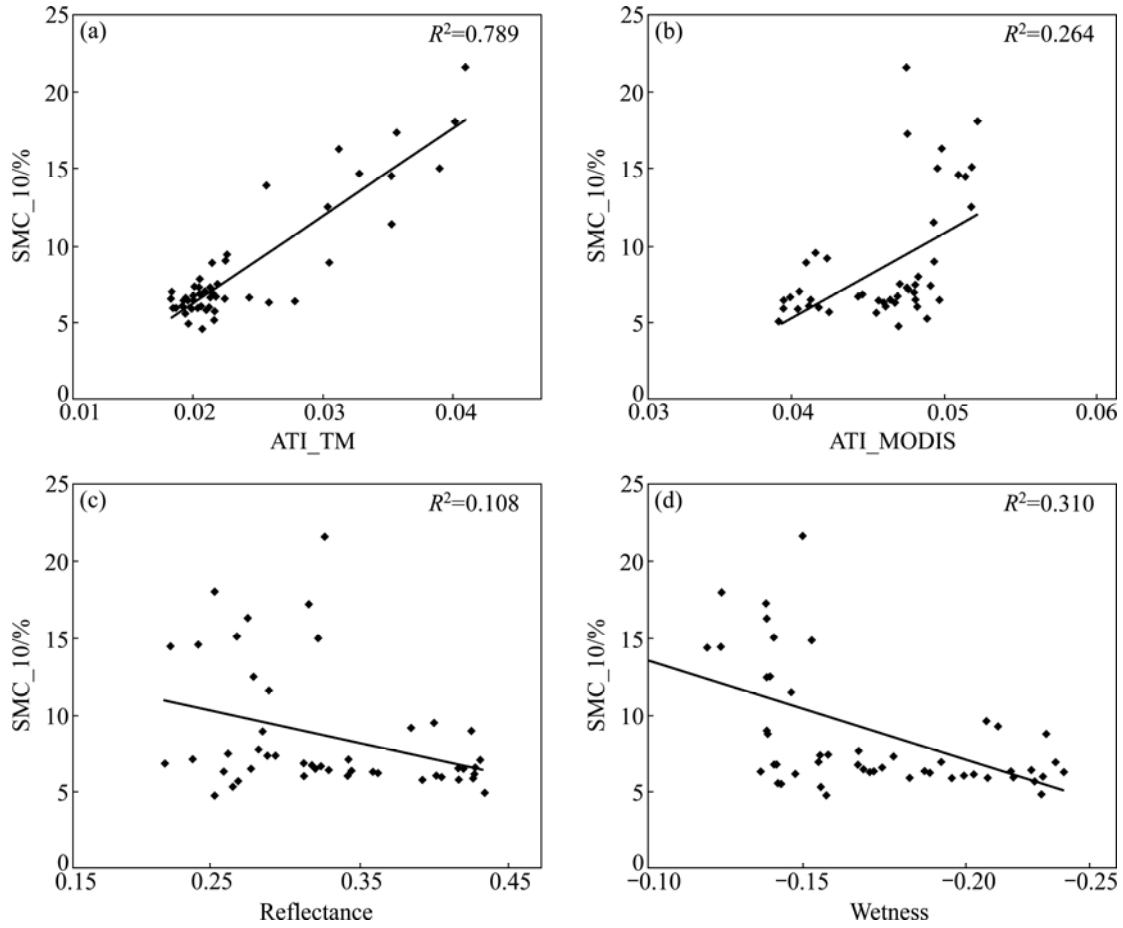

Fig. 7 Correlations of soil moisture vs ATI_TM (a), ATI_MODIS (b), reflectance (c), and wetness index (d)

Table 1 Correlation of ATI and SMC at depths of 10 cm, 20 cm and 40 cm

Regression model	R^2		
	10 m	20 cm	40 cm
Linear	0.789	0.224	0.066
Logarithm	0.764	0.205	0.050
Power	0.752	0.117	0.011
Exponential	0.763	0.133	0.019

Table 2 Regression models of ATI and SMC at depth of 10 cm

Model	Equation	R^2	RMSE
Linear	η=576.06β−4.787	0.789	1.90%
Logarithm	η=14.96×lnβ+65.34	0.764	2.00%
Exponential	η=2.24e$^{54.17\times\beta}$	0.763	1.92%
Power	η=1717.18$\beta^{1.41}$	0.752	1.97%

RMS error (root mean squared error, a measure of the discrepancy between field measured and estimated values) of 1.90%.

Consequently, the soil moisture content of the study area at depth of 10 cm was estimated using the linear model. The estimation (Fig. 9) is reasonable that the

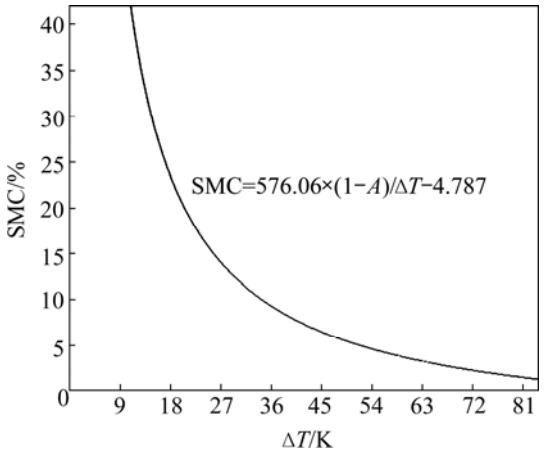

Fig. 8 Correlation between soil moisture (SMC) and soil temperature difference (ΔT)

SMC is lower than 7% in Wulanmulun and Bulianta mines with desert ground surface. Because of the vegetation reconstruction in Daliuta mine, the SMC is higher than the other two mines generally. The cyan color area is nearby the river channel, so the predicted moisture content is very high.

It is worth mentioning that the soil moisture content in the mined area was generally lower than that in the

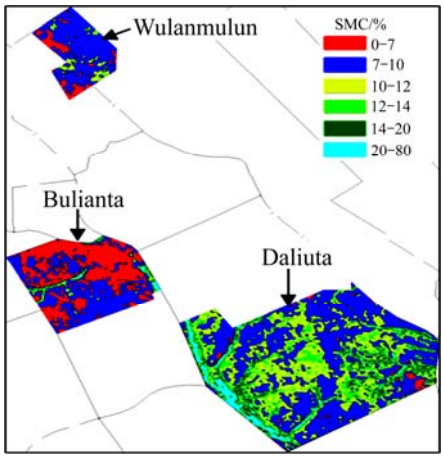

Fig. 9 Estimated soil moisture of study area at 10 cm depth

unmined area, which had also been verified by field investigation [21]. However, there was no difference that could be detected, if using ATI_MODIS obtained only from MODIS without spatial resolution improvement [8]. In general, the accuracy of SMC estimation has been improved. Still, there are some factors that impact the accuracy of the SMC estimation from the soil temperature difference model. For example, the soil temperature difference is simply taken as the difference between the highest and lowest temperature; and the thermal diffusivity should not be taken as a constant, which varies with the soil characteristics.

4 Conclusions

1) Diurnal soil temperature difference is the main constraint for using higher spatial resolution images to calculate soil moisture by ATI. The improved soil temperature difference model can integrate TM/ETM+ and MODIS images to get ΔT at a higher spatial resolution. Thereby, the resolution of ΔT and soil moisture can be enhanced from 1 km to 120 m (TM) or 60 m (ETM+).

2) The improved ATI has a stronger correlation (R^2=0.789) with soil moisture than the wetness index (R^2=0.310), surface reflectance (R^2=0.108) or ATI_MODIS derived only from MODIS images with lower spatial resolution. The RMS error of the estimated soil moisture is lower than 1.90%.

3) The improved soil moisture model is not only suitable for TM/ETM+ images, but also for other higher spatial resolution images with thermal infrared band, e.g. ASTER image or CBERS-1 image.

References

[1] DAI H Y, REN L Y, WANG M, XUE H B. Water distribution extracted from mining subsidence area using Kriging interpolation algorithm [J]. Transactions of Nonferrous Metals Society of China, 2011, 21: s723−s726.

[2] BIAN Z F, LEI S G, INYANG H I, CHANG L Q, ZHANG R C, ZHOU C J, HE X. Integrated method of RS and GPR for monitoring the changes of soil moisture and ground water environment due to underground coal mining [J]. Environmental Geology, 2009, 57(1): 131−142.

[3] WANG L, QU J J, ZHANG S, HAO X, DASGUPTA S. Soil moisture estimation using MODIS and ground measurements in eastern China [J]. International Journal of Remote Sensing, 2007, 28(6): 1413−1418.

[4] PRICE J C. On the analysis of thermal infrared imagery: The limited utility of apparent thermal inertia [J]. Remote Sensing of Environment, 1985, 18(1): 59−73.

[5] MULLER E, DECAMP S H. Modeling soil moisture-reflectance [J], Remote Sensing of Environment, 2000, 76(2): 173−180.

[6] CRUST E P, CICONE R C. Application of the tasseled cap concept to simulated thematic mapper data [J]. Photogrammetric Engineering and Remote Sensing, 1984, 50(3): 343−352.

[7] VERSTRAETEN W W, VEROUSTRAETE F, SANDE C J, GROOTAERS I, FEYEN J. Soil moisture retrieval using thermal inertia, determined with visible and thermal spaceborne data, validated for European forests [J]. Remote Sensing of Environment, 2006, 101(3): 299−314.

[8] CHANG L Q. GIS based remote sensing method for soil moisture reversion and changing disciplination research in mining area: Taking shendong coal mining area as an example [D]. Xuzhou: China University of Mining and Technology, 2006. (in Chinese)

[9] HEJMANOWSKA B, MULARZ S. Integration of multitemporal ERS SAR and Landsat TM data for soil moisture assessment [C]// REMETEY-FÜLÖPP G, CLEVERS J, BEEK K J. Archives of ISPRS Congress XXXIII. Amsterdam: The ISPRS Congress, 2000: 511−518.

[10] PARTON W J. Predicting soil temperatures in a short grass steppe [J]. Soil Science, 1984, 138(2): 93−101.

[11] MINACAPILLI M, CAMMALLERI C, CIRAOLO G, ASARO F D, IOVINO M, MALTESE A. Thermal inertia modeling for soil surface water content estimation: A laboratory experiment [J]. Soil Science Society of America, 2011, 76(1): 1−9.

[12] MA A N. Remote sensing information model [M]. Beijing: Peking University Press, 1997: 41−50. (in Chinese)

[13] ELIAS E A, CICHOTA R, TORRIANI H H, LIER Q. Analytical soil-temperature model correction for temporal variation of daily amplitude [J]. Soil Science Society of America Journal, 2004, 68(3): 784−788.

[14] LEI S G, DANIELS J L, BIAN Z F, WAINAINA N. Improved soil temperature modeling [J]. Environmental Earth Sciences, 2011, 62(6): 1123−1130.

[15] LI D, VOLTERRANI M, CHRISTIANS N E, MINNER D D. Thermal properties of sand based root zone media modified with inorganic soil amendments [J]. Acta Horticulturae ISHS, 2003, 661: 77−85.

[16] QIN Z H, ZHANG M H, ARNON K, PEDRO B. Mono-window algorithm for retrieving land surface temperature from Landsat TM 6 data [J]. Acta Geograph Ica Sinica, 2001, 56(4): 456−466. (in Chinese)

[17] GOETZ S J, HALTHORE R N, HALL F G, MARKHAM B L. Surface temperature retrieval in a temperate grassland with multiresolution sensors [J]. Journal of Geophysical Research, 1995, 100(12): 25397−25410.

[18] QIN Z H, LI W J, ZHANG M H, ARNON K, PEDRO B. Estimating of the essential atmospheric parameters of mono-window algorithm

for land surface temperature retrieval from Landsat TM6 [J]. Remote Sensing For Land & Resource, 2003, 56(2): 37−43. (in Chinese)

[19] GRIEND A A, OWE M. On the relationship between thermal emissivity and the normalized difference vegetation index for natural surface [J]. International Journal of Remote Sensing, 1993, 14(6): 1119−1131.

[20] WANG Z M. MODIS land-surface temperature algorithm theoretical basis document [EB/OL]. 2013−11−12. http://modis.gsfc.nasa.gov/data/atbd/atbd_mod11.pdf.

[21] BIANZ F, LEI S G, CHANG L Q, ZHANG R C. Affecting factors analysis of soil moisture for arid mining area based on TM images [J]. Journal of China Coal Society, 2009, 34(4): 520−525. (in Chinese)

增强分辨率的土壤水表观热惯量法反演

雷少刚[1]，卞正富[1]，John L. DANIELS[2]，刘东烈[3]

1. 中国矿业大学 深部岩土力学与地下工程国家重点实验室，徐州 221116;
2. 北卡罗纳莱纳大学 土木学院，夏洛特 28223，美国;
3. 中国矿业大学 环境与测绘学院，徐州 221116

摘　要：基于热传导理论建立土壤日温差模型，可实现基于 TM 影像提取特定深度的土壤日温差信息。利用该模型获取的土壤日温差与 ATI 的分辨率可达到 120 m (TM)或 60 m (ETM+)。荒漠矿区实验表明，实测土壤水分与 MODIS 得到的 ATI 的相关系数仅为 0.264，而与改进模型得的高分辨率 ATI 相关系数为 0.789，监测的土壤水分均方根误差为 1.90% (m^3/m^3)。提出的方法同样还适用于其他具有热红外波段的高分辨率影像结合 ATI 的土壤水分提取。

关键词：土壤水含量；土壤温差；热惯量；遥感；空间分辨率

(Edited by Sai-qian YUAN)